Electron push-pull effects induced performance promotion in covalent organic polymer thin films-based memristor for neuromorphic application

Panke Zhou [a], Hong Yu [a], Mun Yin Chee [b], Tao Zeng [c], Tianli Jin [b], Hongling Yu [a], Shuo Wu [b], Wen Siang Lew [b,*], Xiong Chen [a,*]

[a] State Key Laboratory of Photocatalysis on Energy and Environment, College of Chemistry, Fuzhou University, Fuzhou 350116, China
[b] School of Physical and Mathematical Sciences, Nanyang Technological University, Singapore 637371, Singapore
[c] Department of Materials Science and Engineering, National University of Singapore, Singapore 117575, Singapore

A B S T R A C T

Covalent organic polymer (COP) thin film-based memristors have generated intensive research interest, but the studies are still in their infancy. Herein, by controlling the content of hydroxyl groups in the aldehyde monomer, Py-COP thin films with different electronic push-pull effects were fabricated bearing distinct memory performances, where the films were prepared by the solid-liquid interface method on the ITO substrates and further fabricated as memory devices with ITO/Py-COPs/Ag architectures. The Py-COP-1-based memory device only exhibited binary memory behavior with an ON/OFF ratio of $1:10^{1.87}$. In contrast, the device based on Py-COP-2 demonstrated ternary memory behavior with an ON/OFF ratio of $1:10^{0.6}:10^{3.1}$ and a ternary yield of 55%. The ternary memory mechanism of the ITO/Py-COP-2/Ag memory device is most likely due to the combination of the trapping of charge carriers and conductive filaments. Interestingly, the Py-COPs-based devices can successfully emulate the synaptic potentiation/depression behavior, clarifying the programmability of these devices in neuromorphic systems. These results suggest that the electronic properties of COPs can be precisely tuned at the molecular level, which provides a promising route for designing multi-level memory devices.

© 2024 Published by Elsevier B.V. on behalf of Chinese Chemical Society and Institute of Materia Medica, Chinese Academy of Medical Sciences.

Covalent organic polymers (COPs) are polymer materials composed of organic molecules linked by covalent bonds through repeating units [1–3]. COPs typically comprise simple organic molecular monomers. They have highly ordered pore structures, and the pore size and shape can be controlled by adjusting the chemical structure of the monomers. COPs have many unique properties, rendering them promising materials for heterogeneous catalysis, gas adsorption and separation, electronic transport, energy storage and conversion [4–12], *etc.* In recent years, neuromorphic applications of memristors, especially those based on COPs materials, hold great promise and significance in the field of artificial intelligence and cognitive computing [13–24]. COP thin films as an information storage medium with structure designability, long-term stability, low power consumption and flexibility have broad application prospects in future information storage scenarios. Besides, COP-based memristors, with their ability to store and update synaptic weights efficiently, mean faster decision-making, quicker response times, and better adaptability to dynamic environments. For instance, Hu and co-authors developed 2D polymer (SL-2DPs) films *via* the gas-liquid interface method and integrated them into flexible memory devices [13]. In another study, Chen *et al.* reported an azulene (Azu)-based 2D conjugated covalent organic framework thin film (COF-Azu) through the solid-liquid interface strategy, which was fabricated as a non-volatile resistive switch memristor [14]. However, the memory performance of these studies is limited to binary behavior, which can no longer meet the requirements for high-capacity data storage in the era of big data. It is an excellent strategy to realize multi-level memory storage by fine-tuning the monomer structures to construct COP thin films with different electronic push-pull interactions. This work demonstrated a novel Py-COPs-based film in situ growth on ITO substrates *via* the solid-liquid interface strategy. Compared to Py-COP-1, the increased content of hydroxyl groups in Py-COP-2 plays a crucial role in achieving multi-level storage behavior. In addition, introducing more hydroxyl groups as an electron acceptor improves the mem-

* Corresponding authors.
E-mail addresses: wensiang@ntu.edu.sg (W.S. Lew), chenxiong987@fzu.edu.cn (X. Chen).
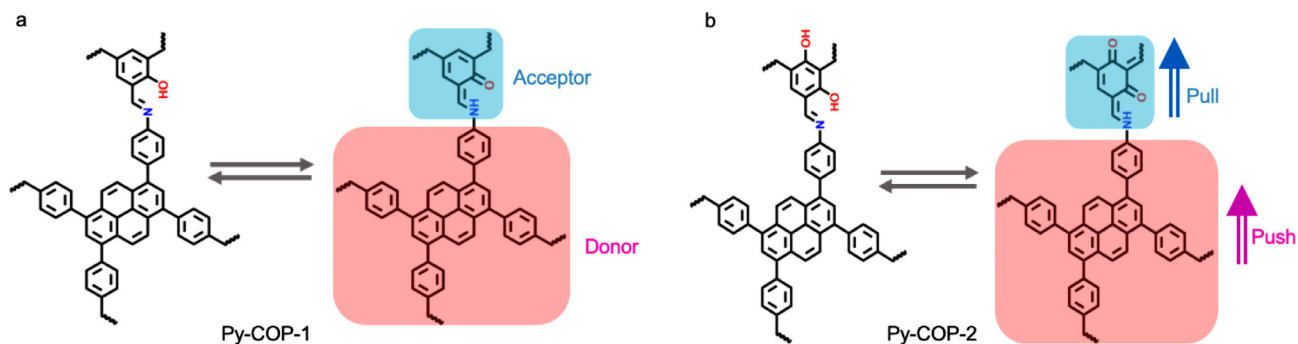
Scheme 1. Partial fragment structures of Py-COP-1 and Py-COP-2.

ory performance through the pull-push effect induced by ketol-enol tautomerism (Scheme 1).

Py-COP thin films were prepared by the condensation of 1,3,6,8-tetrakis(4-aminophenyl)pyrene (PyTTA) and 2-hydroxybenzene-1,3,5-tricarbaldehyde (HTA) or 2,4-dihydroxybenzene-1,3,5-tricarbaldehyde (DHTA) on ITO substrates in a sealed glass tube with mixed solvents at 120 °C for 3 days (Scheme S1 in Supporting information). First, the chemical structure of Py-COP samples was characterized and confirmed by Fourier transform infrared spectroscopy (FT-IR), Raman, solid-state ^{13}C cross-polarization magic angle spinning nuclear magnetic resonance (^{13}C CP-MAS NMR) and X-ray photoelectron spectroscopy (XPS), respectively. Figs. 1a and b show the characteristic stretching bands of the O–H bond (3417–3426 cm^{-1}), C=O (1617–1619 cm^{-1}), C=C (1570–1574 cm^{-1}), and C=N–C (1277–1283 cm^{-1}), indicating the existence of reversible keto-enol tautomerism [25–27]. The Raman spectra show the existence of −C=C and −C=N−C peaks, which is consistent with the FT-IR results (Fig. S1 in Supporting information). The formation of keto-enol tautomerism was also confirmed by ^{13}C CP-MAS NMR and XPS (Figs. 1c and d and Fig. S2 in Supporting information). The peaks at 185.8–189.6 ppm can be attributed to C=O [28,29]. In addition, the presence of C−OH bonds (532.60–532.72 eV) and

C=O bonds (531.25–531.71 eV) signals in the XPS spectra of O 1s of Py-COP-1 and Py-COP-2 provide strong support to the co-existence of keto-form and enol-form tautomers [30]. The amorphous nature of Py-COPs was evidenced by powder X-ray diffraction (PXRD) measurements (Fig. S3 in Supporting information). N$_2$ sorption isotherms were used to evaluate the porous characteristics of the polymers. The Brunauer-Emmett-Teller (BET) values for Py-COP-1 and Py-COP-2 were 604.3 and 676.4 m^2/g, respectively, which indicates microporous polymer network structure (Fig. S4 in Supporting information). The TGA results unveil that Py-COP-1 and Py-COP-2 have favorable thermal stability, which is beneficial for the reliable performance of electronic devices in extreme conditions, such as high temperatures (Fig. S5 in Supporting information).

In order to understand the growth process of the films, we conducted a time-dependent study on the COP films by using SEM (Fig. 2). At the initial stage (after 3 h), SEM images show the formation of crystallites at the substrate interface. At 24 h, the crystallites further aggregate and adhere to the substrate by tight junctions. Fig. 2c illustrates the final form of a continuous film that emerged after 72 h. The dense and smooth surface morphology can be beneficial to inject charge carriers, further improving electron
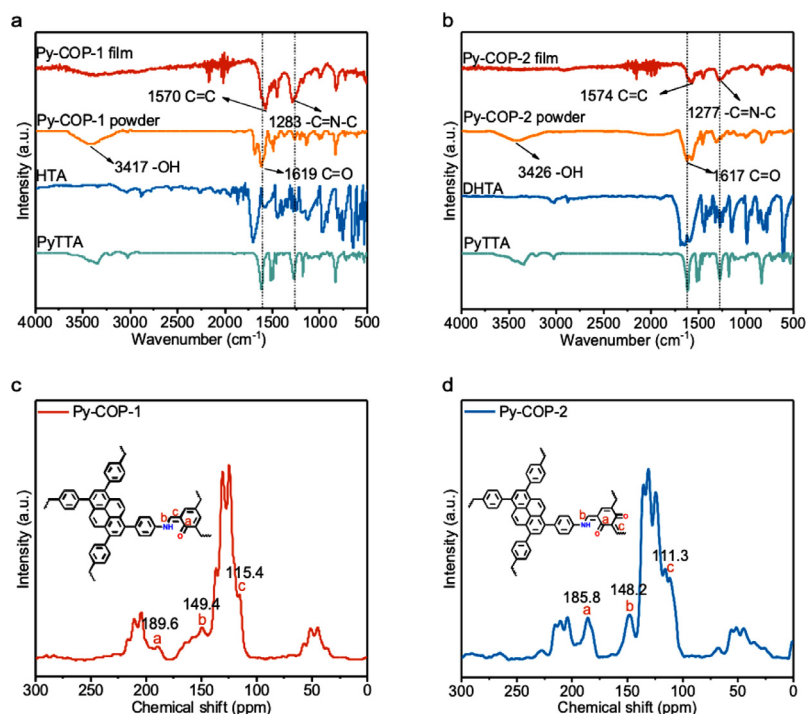
Fig. 1. FT-IR spectra of (a) Py-COP-1 and (b) Py-COP-2. ^{13}C solid-state NMR spectra of (c) Py-COP-1 and (d) Py-COP-2.
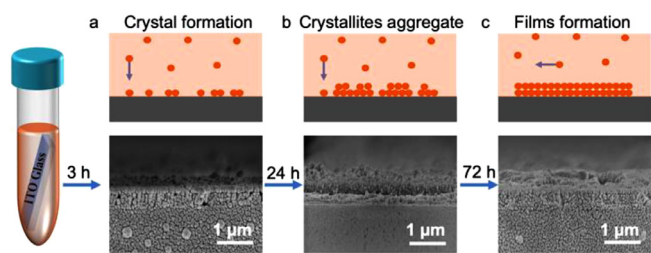
Fig. 2. Cross-sectional SEM images of Py-COP-2 thin films grown on ITO substrates after (a) 3 h, (b) 24 h, and (c) 72 h.

transport performance [31–33]. Figs. S6 and S7 (Supporting information) show the surface morphology of the Py-COP thin films and powders, respectively, revealing the uniform surface for thin films and cluster-like shapes for powders. Due to the increased number of hydroxyl groups in the aldehyde monomer, the water contact angle decreased from 73.6° to 65.8° (Figs. S6a and d). The cross-section SEM images disclosed that the thickness of the Py-COP-1 and Py-COP-2 was approximately 47 nm and 48 nm (Figs. S6b and e), respectively. In addition, the root-mean-square (RMS) roughness of Py-COPs thin films (4.58 nm for Py-COP-1 and 4.86 nm for Py-COP-2 thin films) were confirmed by AFM tests (Figs. S6c and f).

The 3D schematic illustration of the ITO/Py-COPs/Ag memory devices is depicted in Fig. 3a, in which the Ag electrode (~80 nm) was deposited *via* magnetron sputtering. The memory behaviors of Py-COP-1 and Py-COP-2-based devices were assessed by the current-voltage (*I-V*) characteristic curves under the compliance current (CC) of 10 mA (Fig. 3b). For the Py-COP-1-based memory device, the device switched from a high resistive state (HRS, $\sim 1.35 \times 10^{-4}$ A) to a low resistive state (LRS, $\sim 1 \times 10^{-2}$ A) at +1.71 V when the applied sweeping (0 to +3.0 V) voltage increased. It is regarded as the SET process. Then, during the negative voltage sweep (0 to −5.0 V), this device was observed to return from the LRS to the HRS. This is regarded as the RESET process. For the Py-COP-2-based memory device, during the positive voltage sweep (0 to +3.0 V), the two current changes at +0.83 V and +1.32 V

correspond to the intermediate resistive state (IRS) and HRS, respectively. The OFF/ON ratios of the Py-COPs-based devices were $1:10^{1.87}$ (for Py-COP-1) and $1:10^{0.6}:10^{3.1}$ (for Py-COP-2). The endurance of the Py-COPs-based devices shows no clear degradations in the current of the "OFF" and "ON" states at the reading voltage of +0.1 V (Figs. 3c and d). Besides, retention time is essential to evaluate memory device reliability [34,35]. Satisfactorily, these current states of Py-COPs-based devices demonstrate no significant degradation (over 1.0×10^4 s) under a constant voltage of +0.1 V (Figs. 3e and f). Moreover, the resistance distributions of the Py-COPs-based memristors clarify that compared with Py-COP-1, the switching current ratio of Py-COP-2 is increased by an order of magnitude (Fig. 3g), probably due to the effect of the increased content of hydroxyl groups on electron transport and further exhibiting lower conductivity [36,37]. Ternary yield is an indispensable indicator feature for ternary memory devices [38,39]. The ternary yield of these Py-COP-n (*n* = 1, 2) devices (based on 50 devices) is shown in Fig. 3h. For Py-COP-2-based memory devices, the ternary yield (55%) is better than other organic materials-based devices (Table S1 in Supporting information) [13,14,40–45], providing a new idea for developing multi-level storage devices.

The neuronal network in the human brain is functionally connected through synapses, which can realize information memory and learning. Given this, a memristive device similar to the neural synapse structure is possible for neuromorphic computing [46–49]. To this end, the long-term potentiation/depression (LTP/LTD) features of the synaptic plasticity are simulated by applying pulse signals. Fig. 4a shows the change in conductance induced by multiple pulses, where the LTP behavior is achieved by applying +1.8 V/10 µs and the LTD behavior in conductance is achieved by applying −1.8 V/10 µs. These devices can maintain stable ON/OFF states under AC pulse mode (Fig. 4b). As for the fixed pulse width, different LTP/LTD behavior can be attained by adjusting pulse height, suggesting the programmability of the Py-COPs-based devices (Figs. 4c and d).

To understand the electronic properties of Py-COPs film-based memory devices, both ultraviolet photoelectron spectroscopy (UPS) and ultraviolet-visible (UV–vis) absorption measurements were
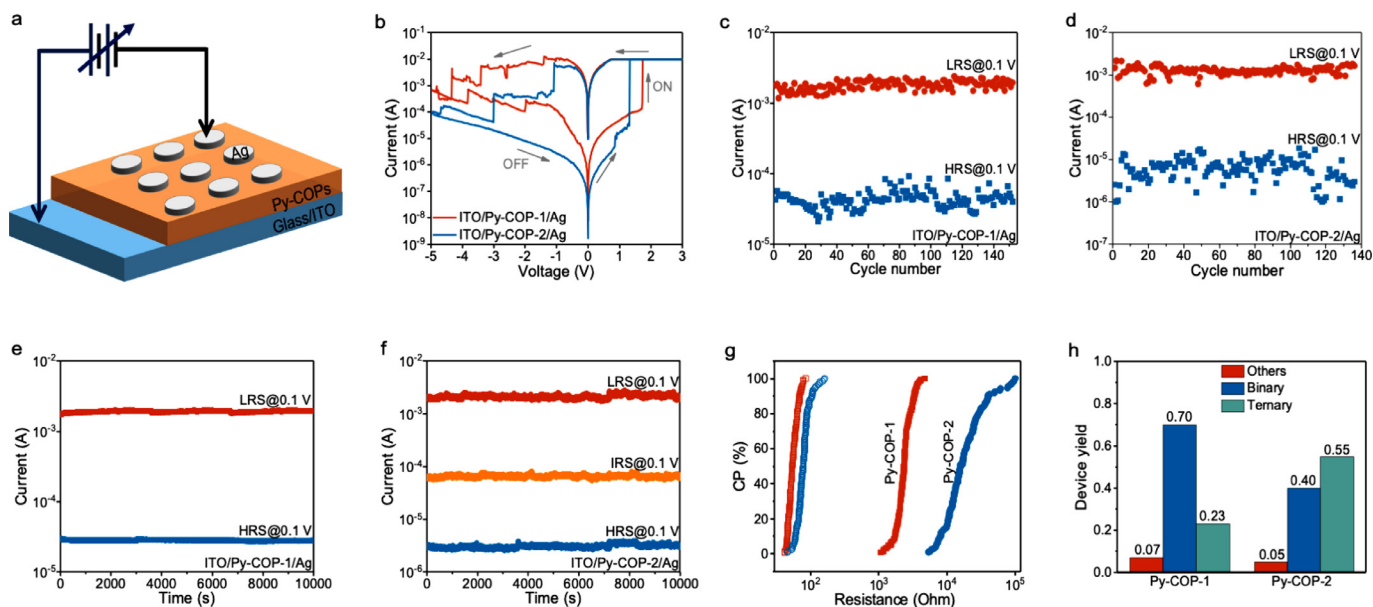

Fig. 3. (a) The 3D schematic diagram of ITO/Py-COPs/Ag devices. (b) *I-V* characteristics of the ITO/Py-COP-1/Ag and ITO/Py-COP-2/Ag memory devices. (c, d) Cycle endurance of the ITO/Py-COP-1/Ag and ITO/Py-COP-2/Ag memory devices showing 152 and 136 cycles, respectively. (e, f) Retention time of ITO/Py-COP-1/Ag and ITO/Py-COP-2/Ag memory device at "OFF" and "ON" states under a constant "read" voltage of +0.1 V. (g) The resistance values cumulative probability of Py-COP-1- and Py-COP-2-based devices. (h) The ternary device yield distributions of Py-COP-1- and Py-COP-2-based devices.
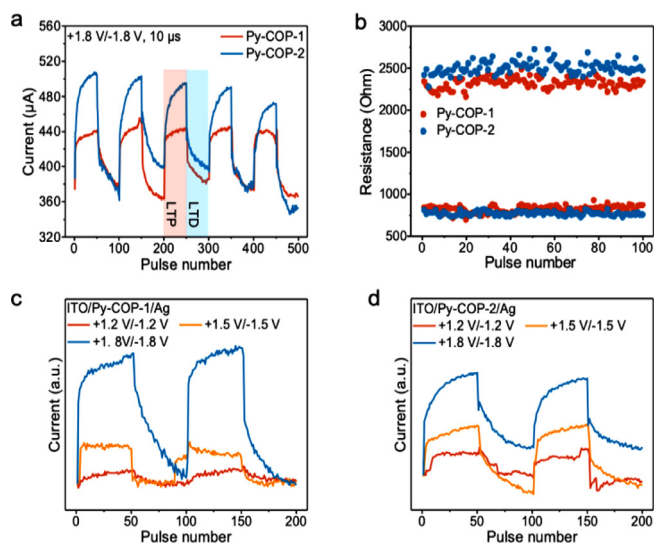
Fig. 4. (a) LTP/LTD behaviors of the Py-COPs-based devices under set pulses (+1.8 V/10 µs) and reset pulses (−1.8 V/10 µs). (b) The endurance characteristics of the Py-COPs-based devices under AC pulse mode. (c, d) The LTP/LTD behaviors of the Py-COPs-based devices under different pulse heights.

Fig. 5. Log-log plot of the *I-V* curves measured of ITO/Py-COPs/Ag devices under positive bias: (a) ITO/Py-COP-1/Ag, (b) ITO/Py-COP-2/Ag. (c) The illustration of the initial, ON1, and ON2 states of the Py-COP-2-based device.

carried out (Fig. S8 in Supporting information). Accordingly, the energy of valence band maximum (E_{VBM}, Figs. S8a and b) [50], band gap (E_g, Fig. S8c), as well as the lowest unoccupied molecular orbital (LUMO) and the highest occupied molecular orbital (HOMO) for these Py-COPs films were estimated, and thus the energy level diagram and carrier transfer process of the devices can be drawn (Fig. S8d). Distinctly, hole injection from the ITO electrode to the hole in HOMO is easier because the ITO electrodes (−4.80 eV) and the HOMO energy levels were less than the Ag electrodes (−4.64 eV) and the LUMO energy levels (Fig. S8d). Therefore, Py-COP-1 and Py-COP-2 were all p-type memory materials where the conductive process of Py-COPs films is dominated by hole injection [51–54]. Moreover, compared with Py-COP-1, the HOMO energy level of Py-COP-2 lowered from −5.29 eV to −5.54 eV, which can be beneficial for hole injection from ITO to HOMO and further effectively reduced the threshold voltages (V_{th}) of devices (Fig. 3b) [34,55].

The conduction switching mechanisms of these Py-COPs-based memory devices can be explained by using the trap-filled limited current (TFLC), the space charge limited current (SCLC) and Ohmic conduction theory, which the *I-V* curves were repainted in the double-logarithmic scale (Figs. 5a and b) [56]. For the Py-COP-1-based memory device (Fig. 5a), the positive sweep region contains three linear regions corresponding to the Ohmic region (slope = 1.19, $I \propto V$), SCLC region (slope = 1.86, $I \propto V^2$) and Ohmic region (slope = 0.96, $I \propto V$), respectively. The SCLC region (slope = 1.86, $I \propto V^2$) was observed due to the carriers captured by the intermediate layer, which promotes the formation of conductive filaments (CFs). For the Py-COP-2-based memory device (Fig. 5b), four different slopes can be observed from *I-V* fitting curve when increasing bias, *i.e.*, Ohmic region (slope = 1.14, $I \propto V$), TFLC region (slope = 2.30, $I \propto V^2$), SCLC region (slope = 2.53, $I \propto V^2$), and Ohmic region (slope = 0.99, $I \propto V$). When an applied voltage reaches the first SET voltage (V_{SET1}), the traps are gradually filled in by the injected carriers (TFLC region, slope = 2.30), which is similar to the conductance behavior of Py-COP-1. Compared with Py-COP-1, the Py-COP-2 thin films can capture more carriers with stronger electron push-pull interactions. Meanwhile, when an applied voltage reaches the second SET voltage (V_{SET2}), CFs may be formed in the Py-COP-2 layer, thus causing the conductance to go directly to the LRS (SCLC region, slope = 2.53). In addition, the drift-diffusion of
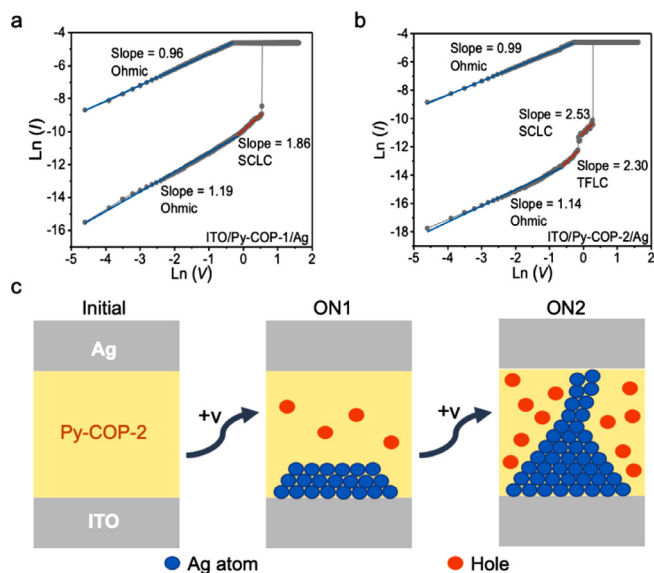
mobile cations is an important way to generate memory behavior, where Cu and Ag are common electrode materials [57]. Fig. 5c shows the model of Ag ions migration to form CFs. During the switching process, the Ag electrode can undergo an electrochemical reaction to afford Ag ions when the external voltage is applied. Then, the Ag ions migrate to form CFs with an increasing electric field. The COPs-based films with different charge trapping capabilities affect the migration rate. Therefore, the ternary memory mechanism of the ITO/Py-COP-2/Ag memory device is most likely due to the combination of the trapping of charge carriers and CFs.

In summary, Py-COP thin films with different electronic push-pull effects were proposed by controlling the content of hydroxyl groups at the molecular level. Py-COP-1 thin films constructed from aldehyde monomers with one hydroxyl group can only exhibit binary memory behavior, while Py-COP-2 thin films prepared from aldehyde monomers with two hydroxyl groups can present ternary memory performance with high ON/OFF ratio ($1:10^{0.6}:10^{3.1}$) and ternary yield (55%). The ternary memory mechanism of the ITO/Py-COP-2/Ag memory device is most likely due to the combination of the trapping of charge carriers and CFs. Specially, these devices also illustrate the synaptic potentiation/depression behavior under pulse mode, proving the possibility of these devices in neuromorphic systems.

Declaration of competing interest

The authors declare that they have no known competing financial interests or personal relationships that could have appeared to influence the work reported in this paper.

Supplementary materials

Supplementary material associated with this article can be found, in the online version, at doi:10.1016/j.cclet.2023.109279.

References

[1] Z. Xiang, D. Cao, L. Dai, Polym. Chem. 6 (2015) 1896–1911.
[2] K. Tan, S. Ghosh, Z. Wang, et al., Nat. Rev. Methods Primers 3 (2023) 1.
[3] D. Yadav, S.K.Awasthi Subodh, Mater. Chem. Front. 6 (2022) 1574–1605.
[4] T. Skorjanc, D. Shetty, M. Valant, ACS Sens. 6 (2021) 1461–1481.
[5] H.A. Patel, S.H. Je, J. Park, et al., Nat. Commun. 4 (2013) 1357.
[6] T. Skorjanc, D. Shetty, A. Trabolsi, Chem 7 (2021) 882–918.
[7] P. Puthiaraj, Y. Lee, S. Zhang, W.S. Ahn, J. Mater. Chem. A 4 (2016) 16288–16311.
[8] C. Zhang, T. Xiao, B. Lu, et al., Small 18 (2022) 2107600.
[9] Z. Ou, B. Liang, Z. Liang, et al., J. Am. Chem. Soc. 144 (2022) 3233–3241.
[10] Y. Cao, W. Sun, C. Guo, et al., ACS Nano 16 (2022) 9830–9842.
[11] P. Peng, Z. Zhou, J. Guo, Z. Xiang, ACS Energy Lett. 2 (2017) 1308–1314.
[12] Z. Xiang, Q. Dai, J. Chen, L. Dai, Adv. Mater. 28 (2016) 6253–6261.
[13] L. Liu, B. Geng, W. Ji, et al., Adv. Mater. 35 (2023) 2208377.
[14] Z. Zhao, M.E. El-Khouly, Q. Che, et al., Angew. Chem. Int. Ed. 62 (2023) e2022172.
[15] D. Wu, Q. Che, H. He, et al., ACS Mater. Lett. 5 (2023) 874–883.
[16] S.W. Park, Z. Liao, B. Ibarlucea, et al., Angew. Chem. Int. Ed. 59 (2020) 8218–8224.
[17] B. Sun, X. Li, T. Feng, et al., ACS Appl. Mater. Interfaces 12 (2020) 51837–51845.
[18] C. Li, D. Li, W. Zhang, H. Li, G. Yu, Angew. Chem. Int. Ed. 60 (2021) 27135–27143.
[19] Y. Song, G. Feng, L. Wu, et al., J. Mater. Chem. C 10 (2022) 2631–2638.
[20] L. Ma, S. Wang, X. Feng, B. Wang, Chin. Chem. Lett. 27 (2016) 1383–1394.
[21] K. Zhou, Z. Jia, Y. Zhou, et al., J. Phys. Chem. Lett. 14 (2023) 7173–7192.
[22] H. Yu, P.K. Zhou, X. Chen, Adv. Funct. Mater. 33 (2023) 2308336.
[23] G.L. Ding, J.Y. Zhao, K. Zhou, et al., Chem. Soc. Rev. 52 (2023) 7071–7136.
[24] P.K. Zhou, H. Yu, W. Huang, et al., Adv. Funct. Mater. 34 (2024) 2306593.
[25] J. Yuan, X. You, N.A. Khan, et al., Nat. Commun. 13 (2022) 3826.
[26] H. Wang, C. Qian, J. Liu, et al., J. Am. Chem. Soc. 142 (2020) 4862–4871.
[27] C. Sun, Y. Zhu, P. Shao, et al., Angew. Chem. Int. Ed. 135 (2023) e202217103.
[28] C.R. DeBlase, K.E. Silberstein, T.T. Truong, H.D. Abruña, W.R. Dichtel, J. Am. Chem. Soc. 135 (2013) 16821–16824.
[29] P. Albacete, J.I. Martínez, X. Li, et al., J. Am. Chem. Soc. 140 (2018) 12922–12929.
[30] C. Liu, W. Wang, M. Zhang, et al., Chem. Eng. J. 430 (2022) 132663.
[31] Y. Zhang, H. Zhuang, Y. Yang, et al., J. Phys. Chem. C 116 (2012) 22832–22839.
[32] P.K. Zhou, L. Zong, K. Song, et al., ACS Appl. Mater. Interfaces 13 (2021) 50350–50357.
[33] X. Zhuang, Y. Chen, G. Liu, et al., Adv. Funct. Mater. 20 (2010) 2916–2922.
[34] Y. Tian, S. Zhu, Y. Di, et al., Dyes Pigm. 186 (2021) 109020.
[35] K. Wang, X. Cheng, W. Xia, et al., J. Organomet. Chem. 983 (2023) 122563.
[36] L. Ai, W. Li, Q. Wang, F. Cui, G. Jiang, ChemCatChem 14 (2022) e202200935.
[37] P. Gu, Y. Ma, J. He, et al., J. Mater. Chem. C 3 (2015) 3167–3172.
[38] Z. Liu, J. He, H. Li, et al., Adv. Electron. Mater. 2 (2016) 1500474.
[39] E. Shi, J. He, H. Zhuang, et al., J. Mater. Chem. C 4 (2016) 2579–2586.
[40] W. Sun, Y. Zhao, J. Zhou, et al., Chem. Eur. J. 25 (2019) 4808–4813.
[41] X. Hou, X. Cheng, J. Zhou, et al., Chem. Eur. J. 23 (2017) 16393–16400.
[42] P.K. Zhou, K. Song, L. Zong, et al., Mater. Today Chem. 25 (2022) 100941.
[43] P.K. Zhou, H. Yu, Y. Li, et al., J. Polym. Sci. (2023), doi:10.1002/pol.20230273.
[44] Y. Liu, Y. Liu, B. Chen, et al., Mater. Today Commun. 33 (2022) 105026.
[45] J. Wang, X. Cheng, W. Qian, et al., J. Mater. Chem. C 8 (2020) 7658–7662.
[46] Z. Wang, H. Xu, X. Li, et al., Adv. Funct. Mater. 22 (2012) 2759–2765.
[47] Q. Xia, J. Yang, Nat. Mater. 18 (2019) 309–323.
[48] L. Liu, P.A. Dananjaya, M.Y. Chee, et al., ACS Appl. Mater. Interfaces 15 (2023) 29287–29296.
[49] D. Wu, Q. Zhang, X. Wang, B. Zhang, Nanoscale 15 (2023) 2726–2733.
[50] Z. Wang, Y. Wang, J. Yu, et al., Nano Lett. 20 (2020) 5562–5569.
[51] S. Liu, P. Wang, Q. Zhao, et al., Adv. Mater. 24 (2012) 2901–2905.
[52] Q. Zhang, J. He, H. Zhuang, et al., Adv. Funct. Mater. 26 (2016) 146–154.
[53] T. Xu, S. Guo, W. Qi, et al., ACS Appl. Mater. Interfaces 12 (2020) 21952–21960.
[54] J. Guo, Y. Zhang, G. Tian, et al., Chem. Eur. J. 27 (2021) 12526–12534.
[55] S. Goswami, A.J. Matula, S.P. Rath, et al., Nat. Mater. 16 (2017) 1216–1224.
[56] P.K. Zhou, X. Lin, H. Yang, et al., J. Alloys Compd. 925 (2022) 166783.
[57] Y. Huang, Z. Zhao, C. Wang, et al., Sci. China Mater. 62 (2019) 1323–1331.